Flow structures stability analysis in a model of a cattle barn using oscillating pattern decomposition method

Štěpán Nosek[1,*], *Zuzana* Kluková[2], *Radka* Kellerová[1], *Michala* Jakubcová[1], and *Zbyněk* Jaňour[1]

[1]Institute of Thermomechanics, Czech Academy of Sciences, Dolejškova 1420/5, 182 00 Praha 8, Czech Republic
[2]Department of Atmospheric Physics, Charles University, V Holešovičkách 747/2, 180 00 Praha 8, Czech Republic

Abstract. A model of a cattle barn and a part-depth atmospheric boundary layer were scaled down to 1:50 to simulate the natural ventilation in a wind tunnel. We studied the impact of three opening configurations (entirely, half and quarterly open, which represented 0.7, 0.35 and 0.17 wall porosity, respectively), on the mean flow and the stability of the flow structures in the barn using time-resolved PIV technique and oscillating pattern decomposition method (OPD). While we observed the most-energy-containing structures (POD modes) in the case of the half opening, the most stable structures (OPD modes) correspond to the fully open case. We found that the stability of the structures increases with the opening width (wall porosity), and the highest frequency of these structures was 11 Hz.

1 Introduction

Naturally ventilated livestock buildings (NVLB), such as a cattle barn, represent one of the most significant sources of ammonia and greenhouse gases emissions. While these emissions pose a severe environmental issue worldwide, the impact of both the outdoor and indoor climatic conditions on these emissions is still not well understood [1].

One of the Environmental parameters governing the ammonia transfer is the type of flow about the manure surface. Previous studies [2–5] observed that the higher is the air velocity and turbulence above the manure surface, the higher is the emission of the ammonia. However, the prediction of such flows inside NVLB is not trivial due to relatively large openings which must ensure the ventilation. This yields in a complex interaction of two types of turbulent flows which is hard to predict and which in turn makes the estimation of ammonia emission from NVLB so difficult.

This study is aimed to shed light on the flows developed within a cattle barn. To do so, we choose the physical modelling of both the outdoor and indoor flows in a wind tunnel since the boundary conditions might be fully controlled and statistically steady. Special attention is paid to model the proper outdoor flow, so-called atmospheric boundary layer (ABL), with all essential flow characteristics such as the mean velocity and turbulence vertical profiles, and integral length scale of turbulence. While the later has never been simulated in previous wind-tunnel studies on NVLB [e.g., 6–9], these studies gave an important insight on the impact of openings configuration on the mean airflow patterns within NVLB. To bring a more in-depth insight into the problem, we captured and analysed the flow structures within a cattle barn model using time-resolved particle image velocimetry (PIV) and oscillating pattern decomposition (OPD) method, respectively. Mainly, the OPD method enables to reveal the "hidden" coherent structures of the flow, which are the most stable (last the longest time in the flow) and how they propagate in space. Compared to Proper Orthogonal Decomposition (POD), OPD gives the information about the frequency at which these structures are excited, and thus which part of turbulence spectra is essential for the flow.

2 Methods

The physical modelling of the interaction of outdoor wind (ABL) with the indoor environment of cattle barn was performed in the Environmental wind tunnel of the Institute of Thermomechanics of the Czech Academy of Sciences. The wind tunnel is an open low-speed wind tunnel with cross dimensions of 1.5 m× 1.5m, and the lengths of the development and test sections are 20.5 m and 2m, respectively.

2.1 Cattle barn model

As far as we know, the first rigorous wind-tunnel study on the interaction of ABL with the indoor environment was performed by Cermak et al. [10]. They studied the natural ventilation of building at a scale of 1:25 and found that so-called internal Reynolds number, Re_i (based on the maximum velocity in the room, which is usually equal to the air velocity at the openings, and the

* Corresponding author: nosek@it.cas.cz

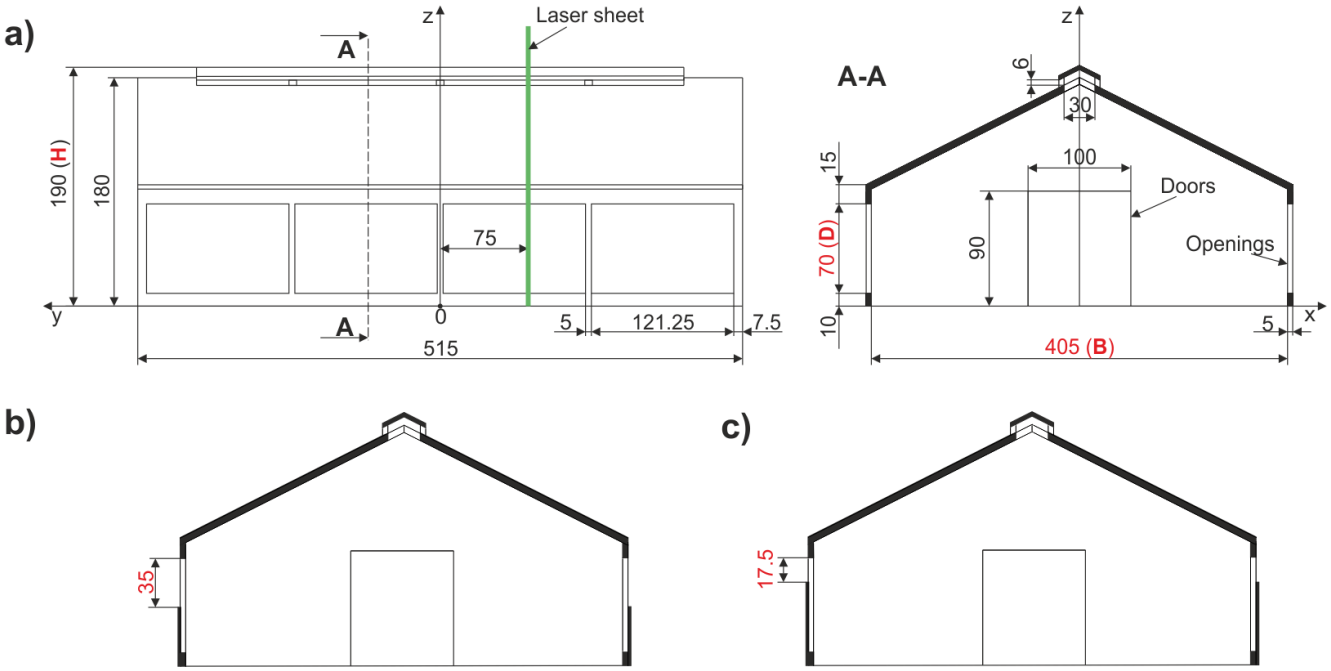

Fig. 1. Sketch of the studied cattle barn model at the scale of 1:50 with respect to the wind-tunnel coordinates: **a)** side view (left) and the cross-section of the cattle barn in the case of the fully open configuration. Cross-sections of the **b)** half and **c)** quarterly open configuration. The doors were left open during the all studied cases. All dimensions are in mm.

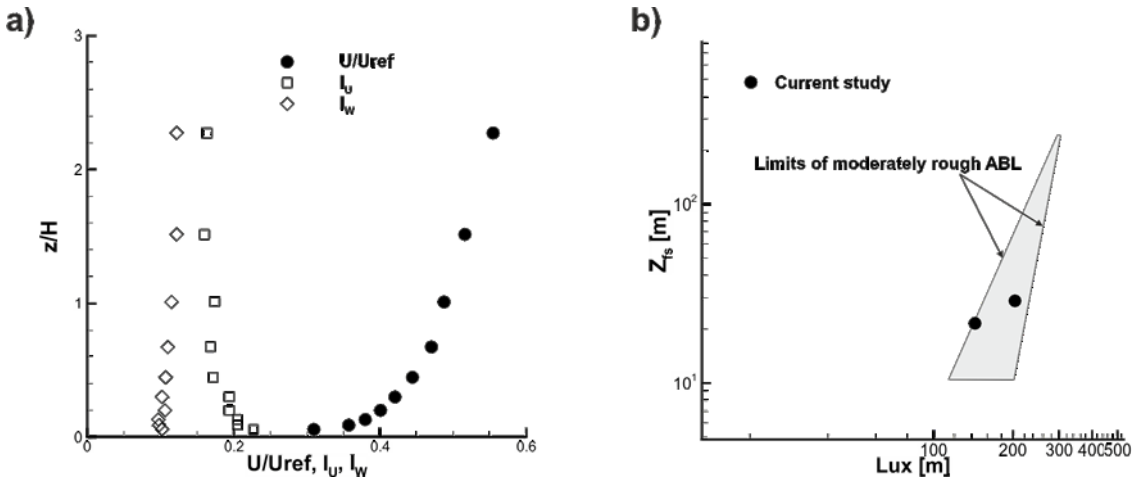

Fig. 2. a) Mean dimensionless vertical profiles of longitudinal velocity (*filled circles*) and longitudinal (*empty squares*) and vertical (*empty diamonds*) turbulence intensity of the simulated ABL; **b)** Comparison of the modelled (*filled circles*) integral length scales of turbulence (L_{ux}) in WT with those (*greyed* area) recommended for moderately rough ABLs by VDI guidelines at full scale.

smallest dimension of the room) should be at least equal to 2×10^4 to ensure the indoor flow independent on Reynolds number. The dimension of the room might be attributed to the inner height of NVLB which was used in this study. Considering Re_i criterion, criteria for ABL modelling in a wind-tunnel and the dimensions of the Environmental wind tunnel, the resulting scale of the cattle barn model yields in 1:50.

The sketch of the model with all important dimensions and all studied configurations is depicted in Fig. 1. The studied configurations reflect three regimes of natural ventilation. The first (Fig. 1a) corresponds to summer, the second (Fig. 1b) to autumn/spring and the third (Fig. 1c) to winter regime. These three regimes also reflect the porosity of the walls (0.7, 0.35 and 0.175, respectively) oriented perpendicularly to the approach wind. While the model was designed as simple as possible, all the important geometrical features (roof ridge, openings geometry, doors) of a typical cattle barn were reproduced.

2.2 ABL model

Modelling of all important ABL characteristics in a wind tunnel simultaneously is not an easy task. The problem usually begins with matching of integral length (longitudinal) scale of turbulence, L_{ux}, or turbulence spectra. The less the model of ABL is scaled down, the harder is to obtain these length scales in a wind tunnel.

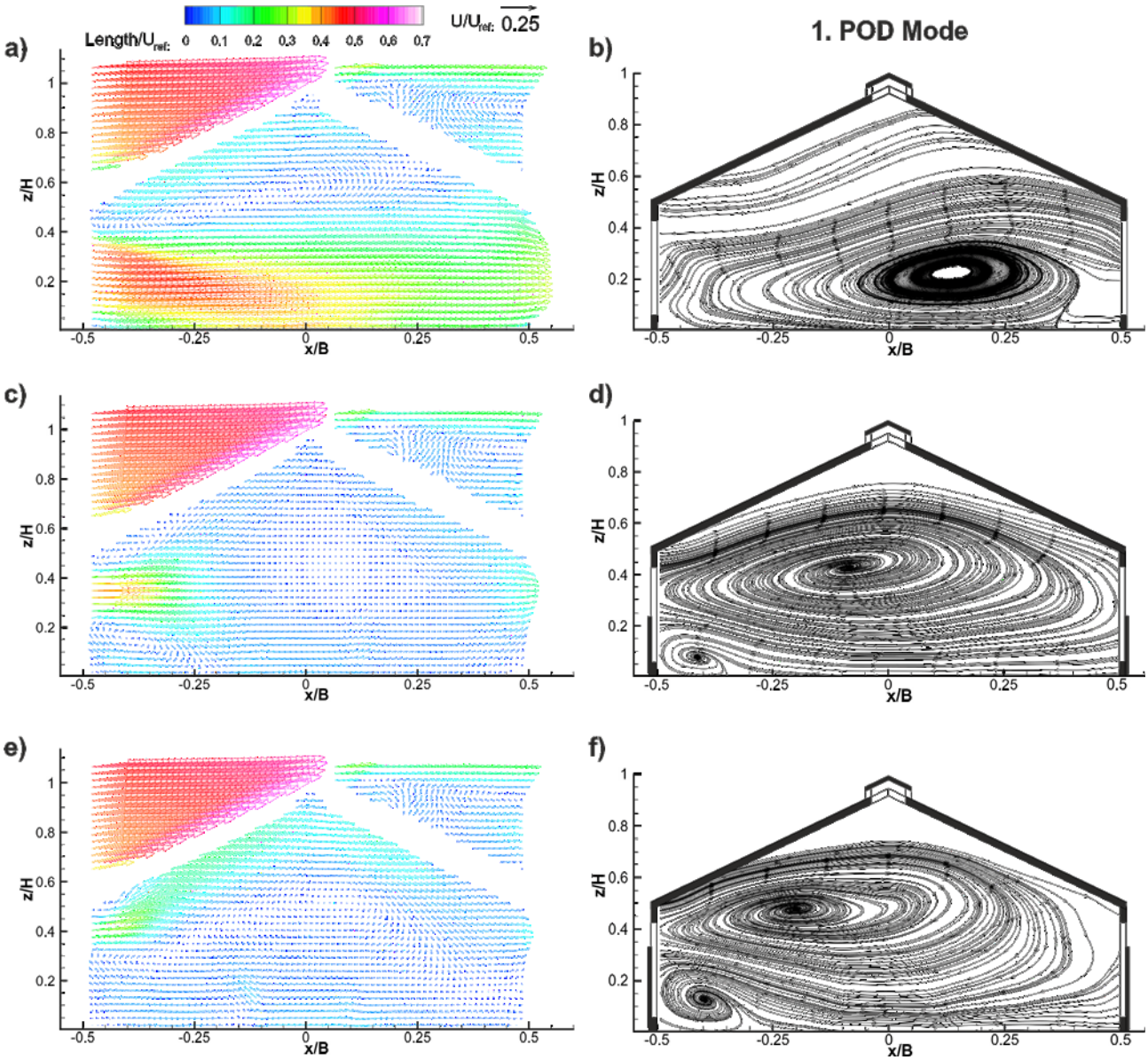

Fig. 3. Mean velocity vector fields (**a,c,e**) and first POD modes (**b,d,f**) for fully (**a,b**), half (**c,d**) and quarterly (**e,f**) open configurations. The colour of the vector corresponds to the dimensionless resultant 2D velocity (*Length/U*$_{ref}$). The dimensionless reference velocity vector (*U/U*$_{ref}$) is depicted in the top right of (a).

Cook [11] show that if L_{ux} and roughness length, z_0, is reproduced in a wind tunnel, a successful simulation of part-depth ABL might be achieved. Such par-depth simulation was also used in the present study since the chosen scale was at the low end of possible scales of the current wind tunnel.

From the velocity and turbulence profiles (Fig. 2a), and integral length scales of turbulence computed for two heights (Fig. 2a) can be clearly seen that the modelled part-depth ABL corresponded those observed for rural (moderately rough) terrains at full scale. The profiles were measured by laser Doppler anemometry 750 mm upstream of the cattle barn model, and hence 250 mm downstream of the last row of turbulent generators. The turbulent generators (thin plates of 50 mm in width and 10 mm in height) covered the bottom of the entire development section (10 m in length) of the wind tunnel in a staggered form. The integral length scale of turbulence was enhanced by vortex generators (spires of 1420 mm in height) at the beginning of the development section.

2.3 Time-resolved PIV setup

A 2D PIV system from Dantec was used at a repetition rate of 200 Hz. The wall-normal streamwise laser sheet from DualPower 30-100 laser was positioned at the middle of the openings (75 mm from the centre of the model, see Fig. 1a) to light particles carried by the flow within the barn at this plane. The particles (about 1 µm in diameter) were continuously injected by a Laskin nozzle generator upstream of the vortex generators. The CMOS camera SpeedSense VEO 410 captured 6227 consecutive images during an acquisition time of 30 s for

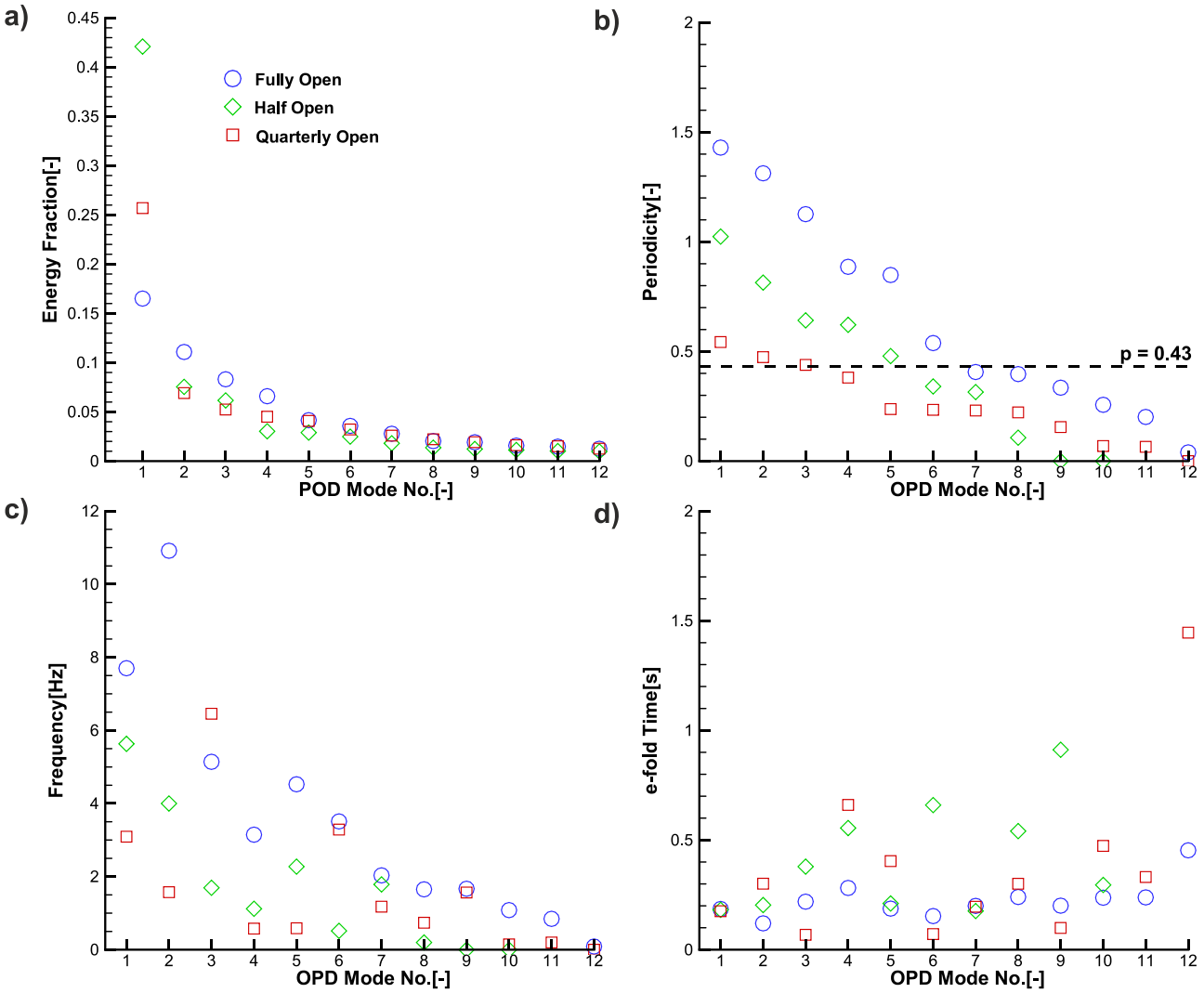

Fig. 4. Computed modes from POD (**a**) and OPD (**b,c,d**) analysis. The dashed line in (b) represents the threshold periodicity (p = 0.43) suggested by Uruba [12].

each studied case. The instantaneous velocity vector fields were computed using Adaptive PIV method by DynamicStudio software. The size of the interrogation area was set to 32×32 pixels with 50% overlap, which resulted in 5 mm (250 mm at full scale) of the spatial resolution of the velocity vector filed.

3 Results

3.1 Mean velocity field

Figs. 3a, 3c and 3e present the mean velocity vector fields computed from all 6227 instantaneous vectors fields for each studied case. The vectors are normalised by the mean free-stream velocity of the wind tunnel, U_{ref}, which was about 5.3 m/s and controlled by Prandtl tube during all runs. The vectors are coloured according to the normalised (by U_{ref}) resulting in 2D velocity.

From Figs. 3a, 3c and 3e one can observe that while within the cattle barn there is a substantial decrease of the velocity with the decrease of the size of the opening, there is no appreciable change in the outdoor flow. However, it should be noted that this insensitivity of the outdoor flow on the cattle barn porosity might not be actual for other areas around the barn due to the three-dimensionality of the studied cases. The lowest internal Reynolds number (Re_i = 22430) corresponds to the quarterly open configuration, but still above the threshold suggested by Cermak et al. [10].

The flow patterns within the barn differ from each case. The fully open configuration (Fig. 3a) enables the outdoor wind blows with ease through the barn to the outlet opening. This blow produces the incoming jet at the lower part of the barn and an anticlockwise-rotating vortex at the upper part. The similar pattern has been observed by Shen et al. [13], although their model of cattle barn was without the ridge openings and open doors.

In the case of the half-open configuration, the anticlockwise vortex is suppressed close to the inlet, and a new, smaller, clockwise vortex is generated just behind

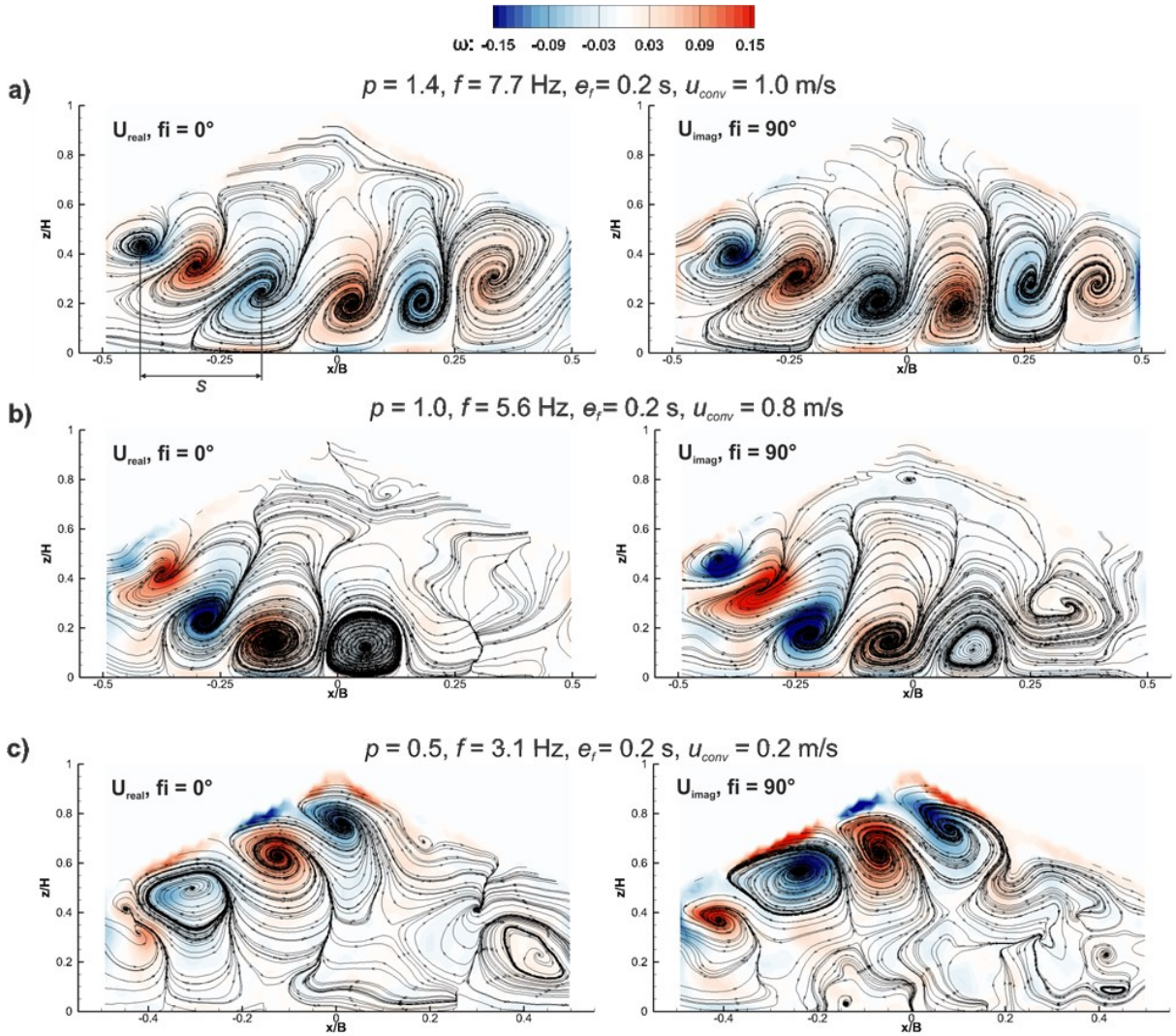

Fig. 5. Spatial OPD modes of the **a)** fully, **b)** half and **c)** quarterly open configuration having the highest periodicity. The first and second column represents real ($\varphi = 0°$) and imaginary ($\varphi = 90°$) part of these modes, respectively. The contours represent the vorticity computed from these parts. The structures' spacing is denoted by *s*.

the wall of the halved inlet opening (Fig. 3c). These two vortices are the result of the shear layers produced at the upper and lower edge of the incoming jet. For the quarterly open case (Fig. 3e), the incoming flow attaches to the roof and the well-known Coanda effect can be observed due to the higher static pressure in the middle of the barn. Such a flow attachment was reported by Morsing et al. [7]. Further downstream, the flow falls to the model bottom and reverses back to the inlet wall, producing a weak anticlockwise vortex in the middle of the barn.

3.2 Flow structures stability analysis

To analyse the dynamics of the flow structures, which are "hidden" due to the chaotic nature of turbulence, we applied the oscillation pattern decomposition (OPD) method. The OPD is based on the idea that complex dynamical systems of many degrees of freedom (such as turbulent flow) might be reduced to more simple dynamical models. Such reduced dynamical model, based on linear algebra, was in climatology introduced by Hasselmann [14] as Principal Oscillation Patterns (POPs). Simply speaking, the OPD method extends the POPs in the way that OPD can resolve standing oscillations [15]. Due to solving the eigenvalue problem embodied in so-called Fokker–Planck equation, the OPD modes consist of complex eigenvalues and complex eigenvectors [12]. While the complex eigenvectors reveal the OPD mode topology, the complex eigenvalue defines the frequency, *f,* and time (so-called e-fold time, τ_e) at which the amplitude of the oscillation decays to $1/e$ [16]. The most stable dynamic structures decomposed from the instantaneous flow filed are those which have the highest periodicity, $p = f.\ \tau_e$. Indeed, the e-fold time is the crucial parameter here, but if there is no oscillation ($f = 0$), there is no dynamics, and hence, in that case, the e-fold time characterises a pulsating structure without any propagation in space. Uruba [12] proposed the threshold value of $p = 0.43$, which means that bellow this value the OPD mode amplitude decays more than by factor 10 during the period, and hence a non-oscillating rapidly decaying mode is detected in the flow.

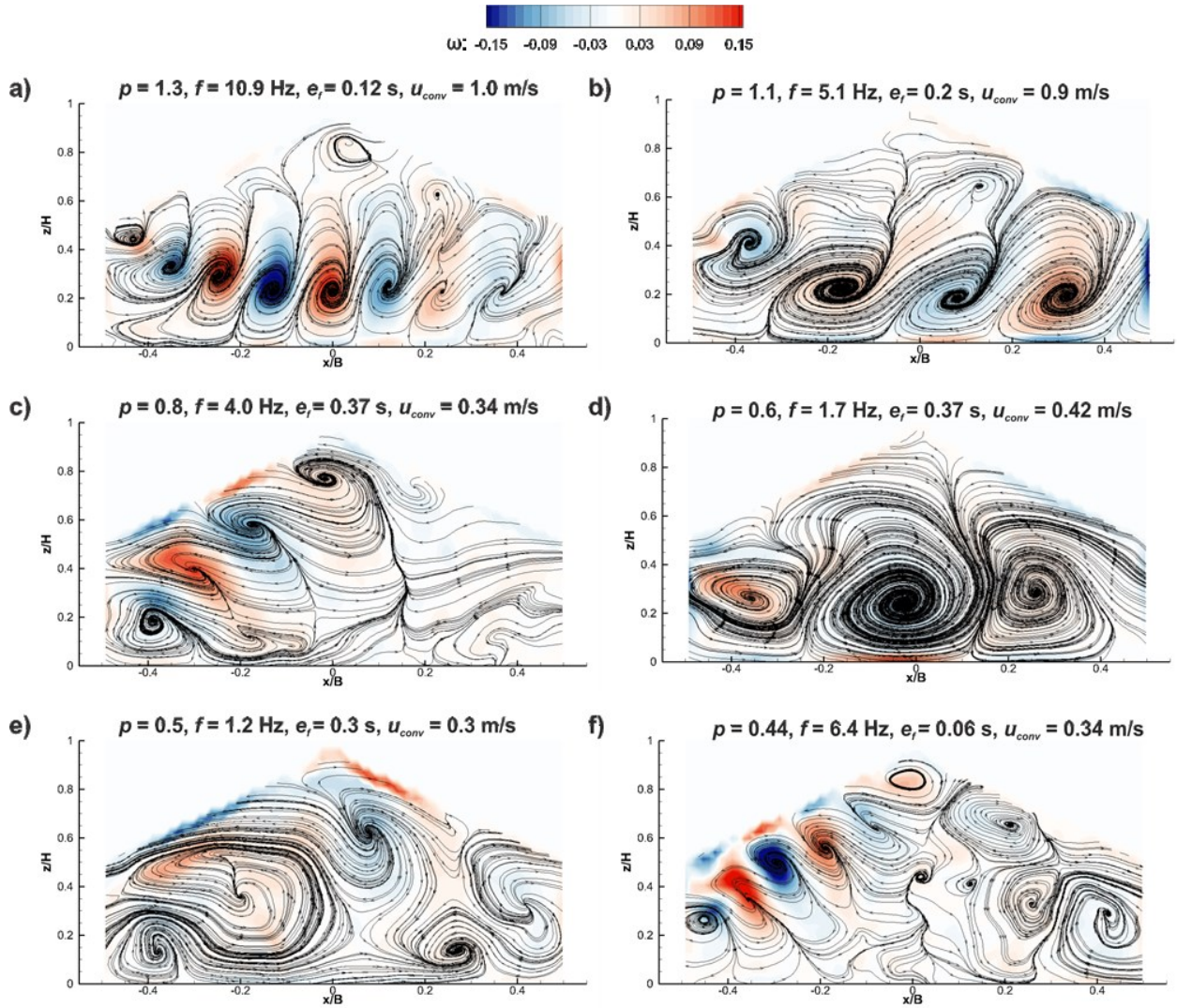

Fig. 6. Spatial OPD modes of the fully (**a,b**), half (**c,d**) and quarterly (**e,f**) opened configuration having the second (**a,c,e**) and third (**b,d,f**) highest periodicity. Only the real parts of the OPD modes at phase 0 are presented for the sake of brevity.

For the OPD analysis, we used DynamicStudio software. Due to saving the computational time, this software computes the OPD eigenvectors and eigenvalues from the already computed "topos" and "chronos" by Proper Orthogonal Decomposition (POD), or more generally by Bi-orthogonal Decomposition (BOD) [17]. Therefore, we also present these POD modes, which are ranked according to their contribution to the total turbulent kinetic energy of the flow filed and compare them with those from the OPD analysis (Fig. 4). The OPD analysis was set to compute all the POD modes which have energy fraction higher than 0.005.

The comparison of the POD (Fig. 4a) with OPD (Fig. 4b) modes shows that the rankings of the primary modes differ concerning the studied case. While the most energetic structures (the first POD mode, Fig. 4a) have been found for the halved opening, the most stables structures (the first OPD mode, Fig. 4b) correspond to the fully open configuration (the same result was obtained for the higher or lower energy fraction setting of OPD). There is no impact of the studied case on those modes (both POD and OPD) which are lower than 11th position of the ranking. However, an appreciable (p > 0.43) structure stability can be observed only for those modes which are higher than 7th (full opening), 6th (half opening), and 4th (quarter opening) position of the OPD ranking.

Fig. 4c shows that the highest frequency at which the structures are excited is about 11 Hz and was detected for the fully open case. With the increase of the OPD modes the frequency generally decreases. The opposite is true for the e-fold time (Fig. 4d). Interestingly, the most stable structures (1 OPD modes) have relatively very short e-fold time which is the same for each studied case, and hence the frequency is the key parameter which drives the stability/dynamics of these structures. Generally, the bigger is the opening, the higher frequency is excited.

For the sake of brevity, we compare the spatiality of the most dominant POD (Figs. 3b, 3d and 3f) and OPD (Fig. 5) modes only. From the first glance of view, one can observe the absolute difference in the spatiality between the POD and OPD modes. The most energetic structures form one (the fully open case, Fig, 3b) or maximum of two (the half, Fig. 3d, and quarterly open case, Fig. 3f) vortices. The most stable dynamic structures have at least four vortices and are more dependent on the studied case (Fig. 5). However, the sizes of these vortices

remain approx. the same for each studied case. They propagate from the inlet opening to the outlet, but only in the case of the fully open configuration the vortices are also presented at the outlet opening, thus do not vanish across the entire barn width. The angle of the direction propagation is the same (approx. -30°) for both the full (Figs. 5a and 5b) and half (Figs. 5c and 5d) openings but changes about 60° (to approx. 30°) in the case of the quarter opening. The convective velocity of the vortices (computed according to [12] from the structures' spacing, s, and frequency, f, as $v = sf$) decreases with the decrease of the opening width.

The second (Figs. 6a, 6c, and 6e) and third (Figs. 6b, 6d, and 6f) OPD modes demonstrate the impact of the excitation frequency on the spatiality of the structures. The higher is the frequency, the more and smaller vortices are excited, and the higher is their convective velocity.

4 Conclusions

In this study, we demonstrate the importance of the stability analysis of turbulent flow within a model of a naturally ventilated cattle barn. The comparison between the studied cases shows that the most energy-containing structures are ranked differently than the most stable dynamic structures. Specifically, the most energetic (POD) mode has been found for the halved opening, while the most stable dynamic (OPD) mode corresponded to the fully open case. Generally, the higher is the opening width, the higher is the stability of the dynamic structures.

The OPD detected the highest excitation frequency of the dynamic structures about 11 Hz from all studied cases. Considering the Nyquist criterion, this suggests that the sampling frequency about 35 Hz should be satisfactory to provide time-resolved data for such studied case and scale ratio. Interestingly, while both the number and convective velocity of the structures increased with the increase of the opening width, the decay time and size of the most stable dynamic structures was independent of the opening width.

Acknowledgement

The authors gratefully acknowledge funding from the Ministry of Education, Youth and Sports of CR (LTC18070) and from the institutional support RVO:61388998. Authors also would like to thank prof. Vaclav Uruba for his consultations to OPD analysis, and Jan Kozohorsky for his valuable support during the experiments.

References

1. B. Bjerg et al., "Review Modelling of ammonia emissions from naturally ventilated livestock buildings. Part 1 : Ammonia release modelling," Biosyst. Eng., vol. 116, no. 3, pp. 232–245, 2013.
2. J. Arogo, R. H. Zhang, G. L. Riskowski, and D. L. Day, "Mass transfer coefficient for hydrogen sulfide emission from aqueous solutions and liquid swine manure," Trans. ASABE, vol. 42, no. 3, pp. 1455–1462, 1999.
3. L. Rong, P. V. Nielsen, and G. Zhang, "Effects of airflow and liquid temperature on ammonia mass transfer above an emission surface: Experimental study on emission rate," Bioresour. Technol., vol. 100, no. 20, pp. 4654–4661, 2009.
4. J. Olesen and S. Sommer, "Modeling effects of wind-speed and surface cover on ammonia volatilization from stored pig slurry," Atmos. Environ. Part a-General Top., vol. 27, no. 16, pp. 2567–2574, 1993.
5. M. De Paepe, J. G. Pieters, L. B. Mendes, S. Van Weyenberg, B. Merci, and P. Demeyer, "Wind tunnel study of ammonia transfer from a manure pit fitted with a dairy cattle slatted floor," Environ. Technol. (United Kingdom), vol. 37, no. 2, pp. 202–215, 2016.
6. Y. Choiniere, F. Blais, and J. Munroe, "A wind tunnel study of airflow patterns in a naturally ventilated building," Can. Agri. Eng, pp. 293–297, 1988.
7. S. Morsing, A. Ikeguchi, J. C. Bennetsen, J. S. Strøm, P. Ravn, and L. Okushima, "Wind induced isothermal airflow patterns in a scale model of a naturally ventilated swine barn with cathedral ceiling," Appl. Eng. Agric., vol. 18, no. 1, pp. 97–101, 2002.
8. M. De Paepe, J. G. Pieters, W. M. Cornelis, D. Gabriels, B. Merci, and P. Demeyer, "Airflow measurements in and around scale model cattle barns in a wind tunnel: Effect of ventilation opening height," Biosyst. Eng., vol. 113, no. 1, pp. 22–32, 2012.
[9] Q. Yi et al., "Wind tunnel investigations of sidewall opening effects on indoor airflows of a cross-ventilated dairy building," Energy Build., vol. 175, pp. 163–172, 2018.
10. J. E. Cermak, M. Poreh, J. A. Peterka, and S. S. Ayad, "Wind tunnel investigations of natural ventilation," J. Transp. Eng., vol. 110, no. 1, pp. 67–79, 1984.
11. N. J. Cook, "On simulating the lower third of the urban adiabatic boundary layer in a wind tunnel," Atmos. Environ., vol. 7, no. 7, pp. 691–705, 1973.
12. V. Uruba, "Near wake dynamics around a vibrating airfoil by means of PIV and Oscillation Pattern Decomposition at Reynolds number," J. Fluids Struct., vol. 55, pp. 372–383, 2015.
13. X. Shen, R. Su, G. K. Ntinas, and G. Zhang, "Influence of sidewall openings on air change rate and airflow conditions inside and outside low-rise naturally ventilated buildings," Energy Build., vol. 130, pp. 453–464, 2016.
14. K. Hasselmann, "PIPs and POPs: The Reduction of Complex Dynamical Systems Using Principal Interaction and Oscillation Patterns," J. Geophys. Res., vol. 93, 1988.
15. V. Uruba, "Decomposition methods in turbulence research," in EPJ Web of Conferences, 2012, vol. 25.
16. V. Uruba and P. Procházka, "On interpretation of spatiotemporal data decomposition," in 15th International Conference on Fluid Control, Measurements and Visualization, 2019, no. May, pp. 1–11.
17. V. Uruba, "Energy and Entropy in Turbulence Decompositions," 2019.